1993A&A...271..381B

Astron. Astrophys. 271, 381–390 (1993)

ASTRONOMY AND ASTROPHYSICS

X-ray emission and temperature profiles for optically selected models of elliptical galaxies

G. Bertin[1], **E. Pignatelli**[1⋆], **and R.P. Saglia**[2]

[1] Scuola Normale Superiore, I-56100 Pisa, Italy
[2] Landessternwarte, W-6900 Heidelberg, Germany

Received May 25, accepted December 4, 1992

Abstract. The main goal of this paper is to determine for a given galaxy to what extent its X-ray emission properties can restrict the class of mass models that is selected by its stellar dynamics. Here we focus on NGC 4472, for which the currently available stellar dynamical data extend out to $\approx R_e$, while the X-ray data sample the region out to $\approx 7R_e$. We show that both the best fit stellar dynamical model that can be proposed without invoking the presence of dark matter with $M/L_B \approx 7.2$ (which is actually judged to be not acceptable in a χ^2-analysis) and the model that, within a 3σ confidence level, contains the largest amount of dark matter in diffuse form ($M/L_B \approx 47$, $M_D \approx 7M_L$, $r_D \approx 7r_L$) lead to remarkably similar X-ray emission and temperature profiles, when such emission is described by means of one standard set of steady-state cooling flow equations. We have also performed a semi-empirical test where the density distribution of the gas is *assumed* (to match in detail the whole X-ray emission profile) and the temperature profiles corresponding to the various optically selected potential wells are inferred from the condition of hydrostatic equilibrium. The basic conclusion remains proved, i.e. that the predicted temperature profiles for models with or without dark matter are very similar to each other.

If the interstellar gas is assumed to have a solar chemical composition and the intracluster pressure is not too high, then the predicted temperature for the models consistent with the stellar dynamical data is close to 1 keV. The emission-weighted temperature is found to be in better agreement with the value of ~ 1.9 keV favored by *Ginga* if a sizable value of the intracluster pressure is assumed.

Key words: galaxies: elliptical – galaxies: structure of – galaxies: individual (NGC 4472) – interstellar medium: kinematics and dynamics of – X-rays: general

Send offprint requests to: G. Bertin
⋆ Postal address: Dip. Astronomia Padova, Italy

1. Introduction

So far the most stringent results on the presence of dark matter in galaxies have been obtained in the context of spiral galaxies, where smooth, symmetric, and extended H I disks are often available as a probe of the gravitational field (see van Albada et al. 1985). The case of elliptical galaxies has been far less clear (see Sancisi & van Albada 1987; Sarazin 1987), mostly because these objects lack the H I disk tracer. Since it is possible to extract direct information only on the amount of matter that is contained inside the sphere defined by the outermost kinematical data-point, a given set of data typically leads to a lower bound to the total mass present. The case of spiral galaxies suggests that dark halos are heavy and diffuse.

The discovery of X-ray emission from early type galaxies initially raised high hopes to give a direct measurement of the mass of these objects, independently of stellar dynamical data which, until recently, could not be sufficiently accurate and radially extended as desired. In fact, for bright ellipticals (in the sense of high X-ray luminosity L_X, see Canizares et al. 1987, hereafter CFT), the X-ray emission is thought to derive from hot interstellar gas, where pressure gradients are expected to balance the overall gravitational field. On this basis, first estimates from *Einstein*'s data gave indications for the presence of very large amounts of dark matter (see Forman et al. 1979; Forman et al. 1985). The main limitation to the use of X-ray emission as a probe of the galactic potential well appeared to be the current difficulty in measuring temperature profiles for the X-ray emitting gas. In many respects, even this lack of information was expected to be not crucial, since theoretical arguments have been proposed to set a lower limit to the mass of an X-ray emitting galaxy (Fabian et al. 1986). In addition, progress is being made on the determination of temperature profiles (Kim et al. 1992). For the specific case of NGC 4472, Thomas (1986) and Loewenstein (1992) conclude that the X-ray data indicate the presence of a massive dark halo. In general, less direct evidence for the presence of considerable amounts of dark matter has also been argued on the basis of evolutionary outflow-inflow

© European Southern Observatory • Provided by the NASA Astrophysics Data System

1993A&A...271..381B

models for the gas dynamics (Loewenstein & Mathews 1987; Ciotti et al. 1991).

On the other hand, caution has been placed in the use of X-ray emission as proof of the existence of heavy halos around ellipticals (CFT; Sarazin & White 1988; Fabbiano 1989), since a conservative interpretation of the data can be shown to lead to fairly low values of the relevant mass-to-light ratios. To be sure, when the behavior of the interstellar gas is studied in detail, many complications and several free parameters are found in the physical picture. Besides the issues of projection effects and of the geometry of the gas distribution (that are often emphasized as a limitation of stellar dynamical models, but apply to gas dynamics as well), non-trivial factors involved are the chemical composition of the gas, the role of the "external pressure" for those ellipticals that are cluster members (and the related issue of "cluster subtraction"), the smoothness of the gas density distribution, supernova rates and heating and gas injection rates, the possible decoupling of cold gas out of the hot interstellar gas ("mass deposition rate"), and the less explored phenomena related to the collective behavior of the hot gas as a plasma.

This paper focuses on NGC 4472, as a test case where good stellar dynamical and X-ray data are available. In contrast to the approach followed by Thomas (1986) and Loewenstein (1992), we impose at the very beginning the severe constraints that are defined by the stellar dynamical data. These constraints on the gravitational potential well, which follow from the greatly improved quality of the velocity dispersion profiles and of the stellar dynamical modeling achieved in the last few years, are firm out to the outermost stellar dynamical point ($\approx R_e$), and leave a range of options for the cumulative total mass $M(r)$ outside R_e, in the region where X-rays are observed. So, we start out from the class of models of the galactic potential well as proposed by stellar dynamics (for which the physics is much simpler!), and then proceed to the calculation of possible X-ray emission and temperature profiles. This approach is expected to lead to two results. On the one hand, since stellar dynamics can usually define only a minimum halo solution for the gravitational potential (see Bertin, Saglia and Stiavelli 1992, hereafter BSS, and Saglia et al. 1992, hereafter SBS), we hope to see from the fit to the more extended (out to $R_X \approx 7R_e$) X-ray emission if a better determination of the amount of dark matter present can be made. This result is achieved by comparing the X-ray profiles calculated for models of the same object with different amounts of dark matter. On the other hand, by confronting the predicted X-ray profiles (as constrained by the choice of optically selected potential wells) with the observations one may hope to narrow down the values of some factors, such as the value of the external pressure p_{ext}, that define the behavior of the X-ray emitting gas.

This program is implemented in two ways. In the first method (see Sect. 2 and 3) we adopt *one standard steady-state cooling flow scenario* in order to predict *both* the *temperature* and the *emission* profiles for the hot gas corresponding to the optically selected stellar dynamical models. In the second, more empirical, approach (Sect. 4), the observed X-ray emission profile is used to infer the gas density distribution and the equation of hydrostatic equilibrium is applied to predict the X-ray temperature profiles for the hot gas corresponding to the optically selected models for the gravitational potential well. In this paper we find (surprisingly) that the predicted profiles turn out to be very close to each other so that X-ray data are bound to give little or no help in clearing off some of the ambiguities intrinsic to the stellar dynamical models. Paradoxically, the most convincing evidence for the presence of a dark halo appears to remain that derived from stellar dynamical studies alone (see SBS).

In this process, the cooling flow model that is adopted *is only one reasonable tool* to predict both temperature and emission profiles. Here we do not enter a critical discussion of the ability of this specific cooling flow scenario to explain in detail the various observed phenomena. In particular, as expected from previous work on the subject, all the X-ray emission (cooling flow) models calculated in the following turn out to be too bright in the inner regions $R < 0.1R_e$, probably because the model used does not take into account the likely loss of hot gas in the central region as a result of rapid cooling (see Sarazin & Ashe 1989); in addition, the predicted X-ray emission profiles at larger radii are somewhat too steep. Different points of view about this issue and about the choice of the relevant cooling flow parameters, such as the supernova rate, have been discussed extensively in recent years and are described in the literature (e.g. see Thomas 1986 and the review by Sarazin 1990). In principle, the first method illustrated in this paper could be applied to less naive forms of cooling flow models, if so desired.

The Appendices summarize some physical properties of the adopted cooling flow model.

2. One standard steady-state cooling flow model, constrained by stellar dynamics

In order to compute both the X-ray emission and temperature profiles for the interstellar gas in an elliptical galaxy, we refer to the standard equations of a spherically symmetric, steady state, "homogeneous" cooling flow model (see Sarazin & White 1987):

$$\frac{1}{r^2}\frac{\mathrm{d}}{\mathrm{d}r}\left(r^2\rho u\right) = \alpha\rho_* \tag{1}$$

$$\alpha\rho_* u + \rho u\frac{\mathrm{d}u}{\mathrm{d}r} + \frac{\mathrm{d}p}{\mathrm{d}r} + \rho\frac{\mathrm{d}\Phi}{\mathrm{d}r} = 0 \tag{2}$$

$$\frac{1}{r^2}\frac{\mathrm{d}}{\mathrm{d}r}\left[r^2\rho u\left(\frac{u^2}{2} + \frac{5}{2}\frac{p}{\rho} + \Phi\right)\right] = -\rho^2\Lambda(T) + \alpha\rho_*\left(\frac{3}{2}\frac{kT_{in}}{\mu m_p} + \Phi\right) \tag{3}$$

that are to be solved for the unknown profiles of the mass density $\rho(r)$, temperature $T(r)$, and radial inflow velocity $u(r) < 0$ of the gas under the appropriate boundary conditions (see below). The equation of state of a perfect gas $p = \rho kT/\mu m_p$ is assumed, where μ is the mean particle mass of the interstellar gas in terms of the proton mass m_p. The stellar dynamical galaxy model

© European Southern Observatory • Provided by the NASA Astrophysics Data System

1993A&A...271..381B

under investigation is specified by three functions, the stellar mass density $\rho_*(r)$, the (averaged in three directions) velocity dispersion of the stars $\sigma_*(r)$, and the total gravitational potential $\Phi(r)$ (we assume that the contribution of the interstellar gas to the gravitational field is negligible). Gas is assumed to be injected in the system by stellar mass loss at a rate $\alpha = \alpha_* + \alpha_{SN}$, where α_{SN} defines the specific contribution of supernovae to the process. The energy balance equation includes a cooling term of the form $\rho^2\Lambda(T)$ which describes radiative losses and a heating term related to the injection of gas at an effective temperature $T_{in} = (\alpha_* T_*(r) + \alpha_{SN} T_{SN})/\alpha$, where the stellar temperature is defined by $kT_*(r) = \mu m_p \sigma_*^2(r)$.

In the following we consider α_*, α_{SN}, T_{SN} and μ to be constant. In particular we take $\alpha_* = 4.7 \cdot 10^{-20}$ sec^{-1}, $\alpha_{SN} = 3.5 \cdot 10^{-22}$ sec^{-1}, $T_{SN} = 4.8 \cdot 10^9$ K, and $\mu = 0.63$ (consistent with a solar chemical composition of the interstellar gas). In addition, since we refer to solar abundances, the cooling function $\Lambda(T)$ is approximated by an analytical expression suggested by Sarazin & White (1987), which is applicable in the temperature range 10^5 K $\leq$ T $\leq 10^8$ K.

The cooling flow equations (1)-(3) are solved under the following boundary conditions: (i) The integration starts from an inner radius called sonic radius r_{son} where the condition $u^2 = 5kT/3\mu m_p$ is imposed. (ii) At such a location the solution is required to be regular. (iii) The mass flow ρu is required to vanish at an outer point called stagnation radius r_{stag}, so that the continuity equation can be rewritten as

$$4\pi r^2 \rho(r) u(r) = \alpha \left(M_*(r) - M_*(r_{stag}) \right) \qquad (4)$$

In contrast with Sarazin & White (1987), we follow the arguments of Vedder et al. (1988), and allow for a divergence in the solution for the temperature $T(r)$ at the outer stagnation point. In this model the value of the pressure at the stagnation point, which remains finite, is identified with the value p_{ext} of the intracluster medium. As explained by Vedder et al. (1988) the use of this boundary condition gives the flexibility to describe the case where the external (intracluster) pressure is fairly high and is equivalent to allowing for a slow little inflow of gas from the cluster. In fact, since the behavior of the temperature profile is obviously unphysical near the stagnation singularity, the proper way to compare this model with the observations is to cut it inside the stagnation radius. At such radius R_{cut}, the pressure is close to the value p_{ext}, but a small inflow of matter is present. In the following, the value of r_{stag} for a given galaxy will be taken to be fixed, $r_{stag} \approx 10 R_e$ (where R_e is the optical effective radius of the galaxy). Then, the choice of the inner sonic radius r_{son} will be adjusted so as to imply a solution with a prescribed external pressure p_{ext}. We have checked that the various profiles remain substantially unaltered for $R \leq 7R_e$ if r_{stag} is pushed out to 15 R_e. In the calculation of the various observational quantities, such as emission averaged temperatures and total X-ray luminosities, we take $R_{cut} \approx 7R_e$.

When a solution for $\rho(r)$ and $T(r)$ is found, the X-ray emission profile is obtained by projecting the emission term of Eq. (3) along the line of sight so that it can be compared with the data from the *Einstein* observatory.

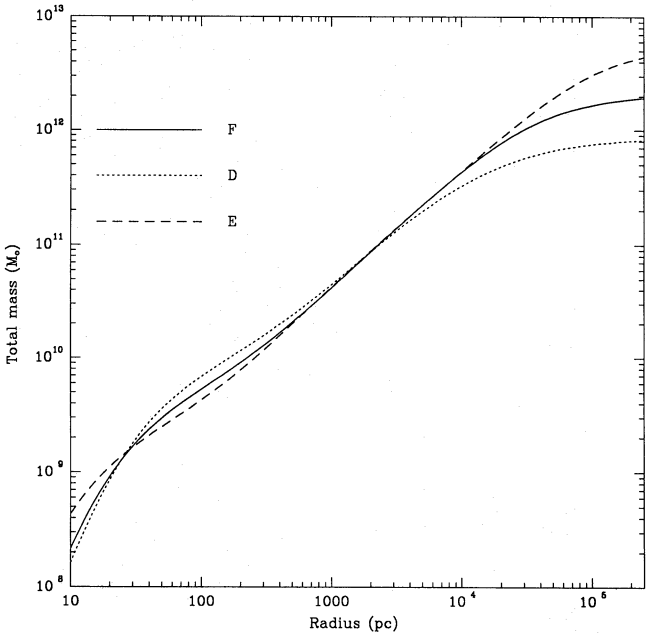

Fig. 1. Total (i.e. dark plus luminous) cumulative mass profiles for the stellar dynamical models D (dotted line), E (dashed line), and F (solid line); see Table 1

The choice of the input stellar dynamical models $\{\rho_*(r),\ \Phi(r),\ \sigma_*(r)\}$ has been made in the following way. We have considered a set of elliptical galaxies with excellent photometric and stellar dynamical data studied previously (SBS), and, in particular, the cases where significant evidence for the presence of dark matter has been found (NGC 4472, NGC 4374, NGC 4636), which turn out to be well known X-ray sources. The analysis of BSS and SBS shows that for each galaxy the class of models $\{\rho_*,\ \Phi,\ \sigma_*\}$ compatible with the stellar dynamical data can be narrowed down considerably. The identified classes of models are made of two-component (luminous + dark matter) self-consistent solutions of the Vlasov-Poisson equations. Note that these are *global* models with *finite* mass. Within the class identified by the stellar dynamical data, the models are very similar to each other out to the outermost available kinematical point; beyond that, they show a range of possibilities corresponding to the presence of smaller or larger halos, as allowed by the stellar dynamical data. In particular, models with too much mass inside $10R_e$ are *excluded* by the available stellar dynamical data on the basis of the physically justified stellar dynamical modeling procedure that has been applied.

The results that we present in this paper refer to NGC 4472. For this galaxy the study of SBS leads to a set of models selected at a 3σ confidence level that all have more mass in the form of dark matter than in the form of stars. The selected models cover a bean-shaped island in the $(r_L/r_D,\ M_L/M_D)$ plane (see Fig. 5 of SBS), where r_L/r_D is the ratio of the half-mass radii of the two components and M_L/M_D is their (total) mass ratio. The best fit model lies roughly at the center of this island. The class of models selected by SBS are based on kinemati-

© European Southern Observatory • Provided by the NASA Astrophysics Data System

1993A&A...271..381B

Table 1. Stellar dynamical models for NGC 4472 (adopted distance: 20 Mpc; adopted stagnation radius: r_{stag} = 100 kpc). Masses are in units of 10^{11} $M_\odot$, mass-to-light ratios are in solar units, lengths are given in kpc. Luminosities are blue luminosities. The last three columns give the values at the stagnation radius, while the second column gives the global value.

Mod	M_D/M_L	r_D/r_L	M_L/L	r_L	M_L	M_D	M/L
D	–	–	7.2	16.7	7.56	–	7.20
E	6.91	7.41	5.9	13.8	6.83	24.7	27.3
F	1.69	2.80	6.5	16.1	6.98	9.78	15.6

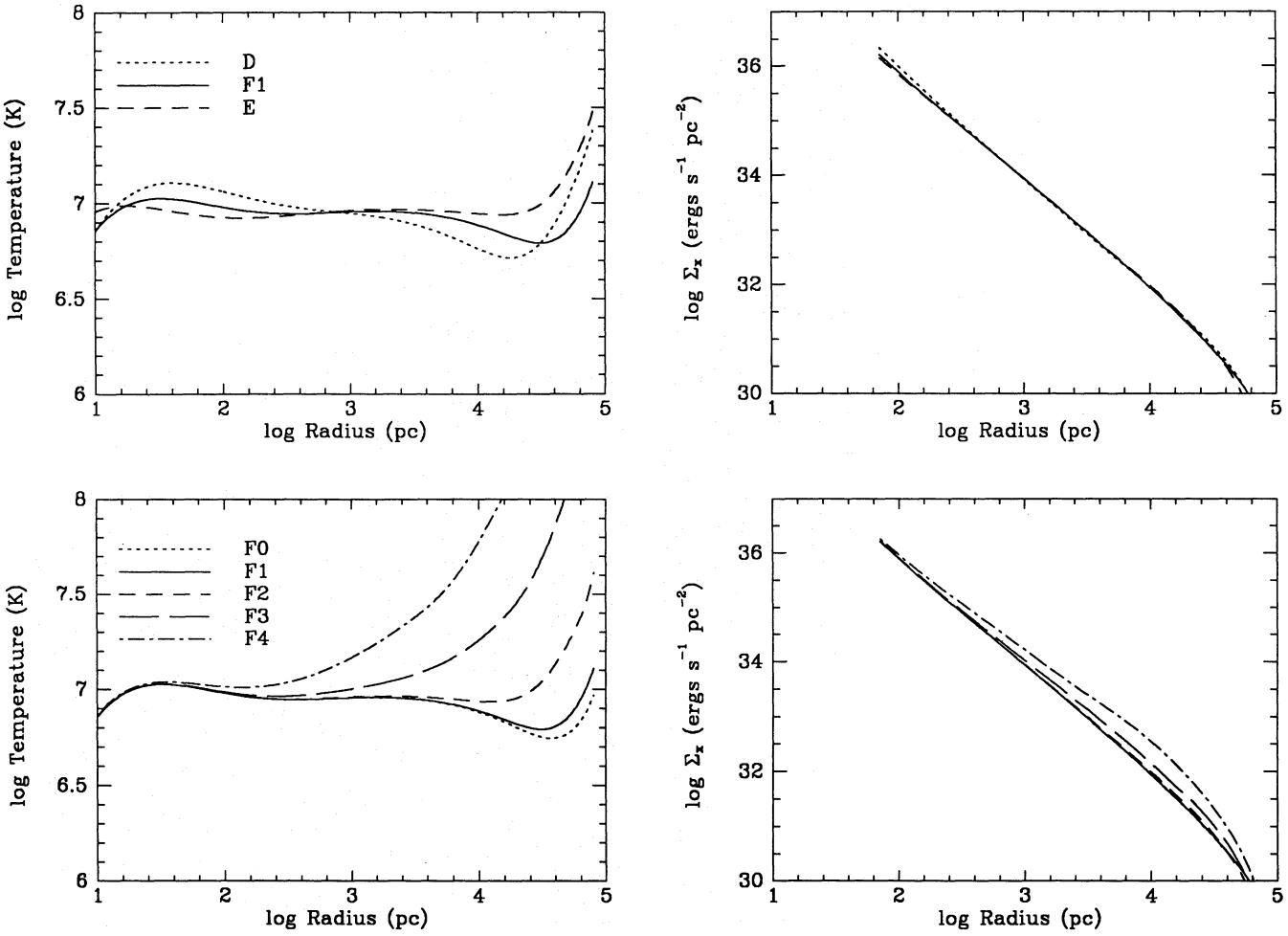

Fig. 2. Radial plots of temperature (left) and X-ray surface brightness (right; as would be seen by the *Einstein* IPC) for some cooling flow models. In the upper frames we show the behavior of the models D, E and F1 (see Table 2) for different amounts of dark matter, but keeping nearly fixed the external pressure, which is in the range 1300-2800 K cm^{-3}. In the lower frames we show the five models F0-F4, obtained by varying the external pressure in the range from 910 to 580000 K cm^{-3}, for the same stellar dynamical model F. The temperature profiles are cut at the radius R_{cut} = 80 kpc

cal data (Davies & Birkinshaw 1988) that sample a sphere of radius R^K_{max} = 64″. Recently, strong support to the results of this modeling has derived from the more extended and accurate dispersion profiles ($R^K_{max} \approx 110'' \approx R_e$) obtained at NTT (see Saglia et al. 1993). Within the 3σ island one notes a wide set of possible options. On one extreme case, the dark halo has only moderate mass ($M_L \approx M_D$) and is not too diffuse ($r_L \approx 0.4 r_D$). On the other extreme, one finds a model with a massive diffuse halo ($M_D \approx 7M_L, r_D \approx 7r_L$; the *global* value for this model is $M/L_B \approx 47$). One goal of this paper is to determine to what extent X-ray data can further constrain the allowed range of models for a galaxy like NGC 4472. In order to answer this question, we focus on three models for NGC 4472 (see Table 1): model D is devoid of dark matter, and corresponds to the best one-component stellar dynamical model available (that would be rejected at a 7σ confidence level). Model E, is the ex-

© European Southern Observatory • Provided by the NASA Astrophysics Data System

1993A&A...271..381B

treme case with maximum amount of dark matter within the 3σ island. Model F, is our favorite best-fit model. The cumulative *total* mass as a function of radius is shown for the three models in Fig. 1. Notice the constraints imposed on the mass models by the stellar dynamical data: inside R_e the models are very similar to each other, and at $r = 80$ kpc, which is the current limit of X-ray observation, we can change the total mass by a factor of 4, but not more than that. In the next section we will determine for these models how the X-ray emission and temperature profiles computed from the solution of the adopted cooling flow equations differ from each other.

3. Predicted X-ray emission and temperature profiles of the adopted cooling flow

In Table 2 we give a summary of the properties of the cooling flow models that have been computed for the optically selected stellar dynamical models of NGC 4472. Several runs for the best fit model F (with dark matter) have been performed in order to explore the dependence of the various profiles on the value of the external pressure p_{ext}. For all the models the adopted stagnation radius is kept fixed at $r_{stag} = 100$ kpc, while the sonic radius falls in the range of 5–10 pc.

Some of the general conclusions that can be drawn on the structure of the cooling flow profiles can be interpreted analytically, as shown in Appendix A. The models follow the main well-known properties of cooling flows already shown by other authors. In particular, all the models are in nearly hydrostatic equilibrium except in the innermost regions (about 30 pc for model F1) where the inflow becomes appreciable. For sufficiently low values of the external pressure, the resulting gas distribution is nearly isothermal, with $T \propto M_L$.

3.1. Models with different amounts of dark matter

In the upper section of Fig. 2 we summarize the properties of the temperature and emission profiles for the models D, E, and F1. The IPC X-ray emission profiles are essentially identical to each other. Minor differences are found in the temperature profiles of the gas; the three profiles are all approximately isothermal in the region from 0.1 kpc to 50 kpc, with $T \approx 10^7$ K, and compare well with the profiles derived from the *Einstein* data (see Fig. 6 of Forman et al. 1985). The flattest temperature profile corresponds to the case where the mass ratio M_D/M_L is largest.

3.2. Models with different amounts of external pressure

A wide range of values for p_{ext}, with a change by a factor of more than 500 between the extreme cases, has been covered. This sequence of F-models shows that cluster induced changes in the cooling flow profiles are more significant than those associated with variation in the dark matter content. Again the temperature profile is the most sensitive. In particular, large external pressures give rise to sizable temperature gradients, so that for the extreme F4 model the gas temperature exceeds 10^8 K outside $r \approx 20$ kpc. These results are illustrated in the lower part of Fig. 2.

3.3. Comparison with the observed X-ray properties

In order to test the merits and the limitations of the adopted cooling flows models, we compared our predicted profiles with the observed X-ray spectral temperature and surface brightness profiles.

3.3.1. Surface brightness profiles

In Fig. 3 we show the X-ray surface brightness profile for the model FF, together with the *Einstein* data for NGC 4472, as given by Trinchieri et al. (1986). The emission profile of the model is found to be in reasonable agreement with the observed data in the region $R > 0.1R_e$, but somewhat too steep. In addition, the model fails at very small radii, where we found a surface brightness up to one order of magnitude higher than that observed (note, however, that the model curve is not convolved as would be required for a fair comparison in the central 10 arcsec, given the resolution of the *Einstein* HRI data). Even though the comparison with the observed emission profile of this model is better than that of Fig. 7 in Sarazin (1990), the fit is not satisfactory. These difficulties with the cooling flow model are well known (e.g. see Sarazin & White 1988), and could probably be explained by relaxing the "homogeneous" assumption (see Sarazin & Ashe 1989) and by taking into account the effects of thermal instabilities (see, e.g. Fabian & Nulsen 1977; Mathews & Bregman 1978; Balbus 1988). Thus the central luminosity peak could be reduced, because much of the gas would cool below X-ray emitting temperatures before flowing into the center of the galaxy. Another way to resolve these difficulties was given by Thomas (1986), who based his analysis on a model with negligible mass injection from normal stellar activity and invoked a very small supernova rate.

3.3.2. Temperature profiles and role of the external pressure

A good determination of the external pressure p_{ext} for a galaxy like NGC 4472 would be possible if we had a good model for the intracluster medium. Such a model, based on the X-ray emission from the cluster, has been developed to fit the data in the vicinity of M87 (Fabricant & Gorenstein 1983); it is not expected to set stringent limits on the intracluster pressure so far away from the center of Virgo, especially because NGC 4472 is near the center of a subcluster, even without taking into account the other limitation posed by the uncertain location of the galaxy within the cluster as a result of projection effects. In fact, the structure of the outer X-ray isophotes suggests that the role of the cluster pressure in the outer regions of the hot gas of NGC 4472 is very important. Thus, we are encouraged to leave the external pressure p_{ext} almost like a free parameter. Even so, we should regard cases F3 and F4 as unrealistic, for which the adopted high values of p_{ext} may turn out to be incompatible with current (see Takano et al. 1989) or future data.

© European Southern Observatory • Provided by the NASA Astrophysics Data System

1993A&A...271..381B

Table 2. Cooling-flow models for the X-ray emission of NGC 4472. We report external pressure, total mass of gas, X-ray luminosity in the *Einstein* band within the stagnation radius for every model, together with the gas parameters at the sonic radius. The last columns give the emission-weighted temperatures.

Model	p_{ext} [a]	M^b_{gas}	L_X [c]	r^d_{son}	$(n)^e_{r_{son}}$	$(u)^f_{r_{son}}$	$(T)^g_{r_{son}}$	$(\dot{M})^h_{r_{son}}$	$\bar{T}^i$	$\bar{T}^j_H$
D	2775	1.91	3.40	7.0875	222	320.8	4.45	1.13	8.48	6.54
E	2840	1.71	3.23	4.935	372	355.6	5.47	1.01	9.45	9.50
F0	913	1.81	3.23	6.761	223	323.2	4.52	1.04	8.21	6.77
F1	1290	1.82	3.25	6.7609	224	323.2	4.52	1.04	8.42	7.01
F2	4700	1.90	3.36	6.760	224	323.2	4.52	1.04	9.98	9.95
FF	15 170	2.17	3.62	6.7575	224	323.3	4.52	1.04	13.9	15.5
F3	55 000	2.63	4.26	6.750	224	323.3	4.53	1.04	26.8	43.4
F4	580 000	4.13	7.89	6.7	227	323.5	4.53	1.04	145	442

[a] K cm^{-3}
[b] $10^{10} M_\odot$
[c] 10^{41} ergs/sec; inside 80 kpc
[d] pc
[e] n = $\rho/\mu m_p$; cm^{-3}
[f] km/sec
[g] 10^6 Kelvin
[h] $M_\odot$/yr
[i] 10^6 Kelvin
[j] 10^6 Kelvin – for the hydrostatic models (see Sect. 4)

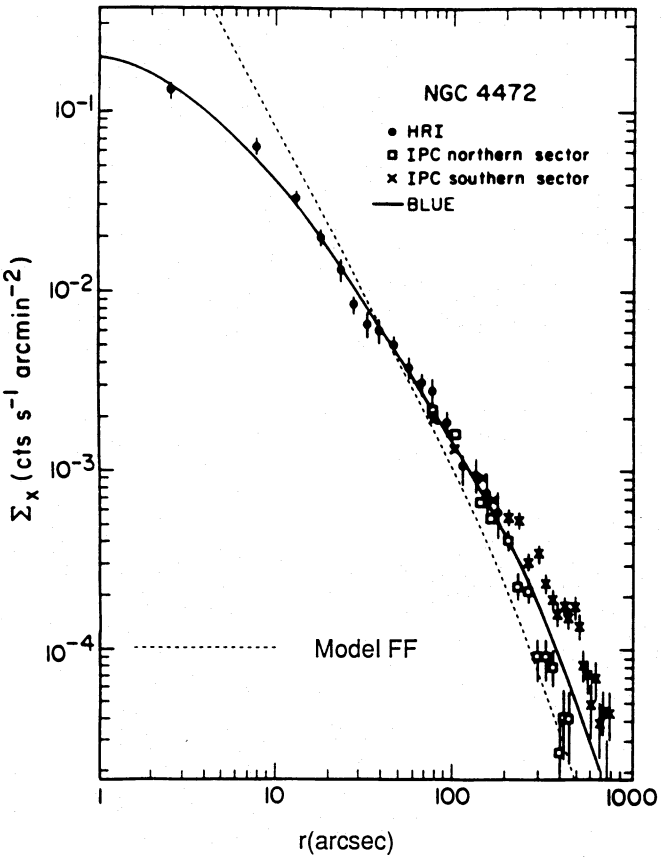

Fig. 3. X-ray surface brightness profiles for the model FF, together with the *Einstein* data for NGC 4472, as given by Trinchieri et al. (1986, Fig. 5). The solid line shows the observed optical luminosity profile (with an arbitrary normalization)

Note that the temperature profile is quite sensitive to the value of the parameter p_{ext} (see Fig. 2). An interesting effect produced by a large value of p_{ext} is to induce a rising temperature profile (see Vedder et al. 1988). Evidence for such a positive gradient has been found recently in some galaxies by Kim et al. (1992). Note that, in some respects, a sizable external pressure can mimick the presence of a large massive halo (see also Fabian et al. 1986; Sarazin & White 1987).

In view of the considerable uncertainties in the current determination of temperature profiles from X-ray observations , we have chosen to quantify the effect in terms of an emission weighted temperature $\bar{T}$, defined as

$$\bar{T} = \frac{\int < \varepsilon(r) T(r) > R\,\mathrm{d}R}{\int < \varepsilon(r) > R\,\mathrm{d}R} \tag{5}$$

where $\varepsilon(r) = \rho^2 \Lambda(T)$, $<>$ indicates projection along the line of sight, and the integrals are performed from the sonic radius to 80 kpc. In general, for given values of the cooling flow parameters for the gas and of the supernova rate, the temperature $\bar{T}$ is a function of the stellar dynamical model $\{\rho_*,\ \Phi,\ \sigma_*\}$ and of the external pressure p_{ext}.

In Table 2 we show the values of $\bar{T}$ for the models of NGC 4472 selected previously. For all the D, E, F1 and F2 models we have $\bar{T} \approx 1$ keV, which agrees with the 0.5–2.0 keV range given by CFT, (the profiles also match the trend derived by Forman et al. 1985) but is at variance with the more recent data from *Ginga* (see Awaki et al. 1991), which has $\bar{T} = 1.9 \pm 0.2$ keV $= (2.1 \pm 0.2) \cdot 10^7$ K. The models with higher values of the boundary pressure are hotter, up to the $\bar{T} \approx 9$ keV for the extreme case F4. For these high-pressure models ($p_{ext} > 10\,000$ K cm^{-3}) $\bar{T}$ is determined by the outer (and hotter) regions of the galaxy,

© European Southern Observatory • Provided by the NASA Astrophysics Data System

1993A&A...271..381B

being nearly insensitive to the variation of the stellar dynamical model adopted. Therefore, one way to reconcile the relatively high temperature reported by *Ginga* for NGC 4472 with the observed velocity dispersion of the stars (which is determined with excellent precision) is to assume that the intracluster medium in the vicinity of such a galaxy has a fairly high pressure ($p_{ext} \approx 30\,000 - 40\,000$ K cm^{-3}).

Finally, we should keep in mind that both the temperature derived from the observed spectra and that predicted by the models are sensitive to the assumed chemical composition of the interstellar gas. Relaxing the assumption of solar abundances can lead to different results. A discussion of these issues goes beyond the scope of the present paper.

4. A different test: hydrostatic models

The fact that the adopted steady-state cooling flow models are quite naive and that in any case the cooling flow would be quite slow over the main body of the galaxy prompted us to make a different test, in order to check the generality of our conclusions.

Since the emission profile is mostly determined by the gas density distribution $\rho(r)$, and reasonably well determined by the observations, we can *assume* a density profile just in order to match the observed X-ray profile. For simplicity, we may refer to the analytical representation of the so called β-models:

$$\rho = \rho_0 \left[1 + \left(\frac{r}{r_0}\right)^2\right]^{-3\beta/2} \tag{6}$$

with $r_0 = 500$ pc and $\beta = 0.5$ as argued by Trinchieri et al. (1986) on the basis of the HRI *Einstein* data. Thus, we can *impose* quasi-hydrostatic equilibrium and derive:

$$T(r) = \frac{\mu m_p}{\rho(r)} \left[G \int_r^{r_{stag}} \frac{M(r')\rho(r')}{r'^2}\,\mathrm{d}r' + p_{ext}\right] \tag{7}$$

where $M(r)$ is taken from the prescribed D, E, F models introduced before. Here r_{stag} is just a reference radius and has no dynamical (inflow) interpretation. The profile $T(r)$ thus determined should be introduced back in the emission profile associated with $\rho^2\Lambda(T)$ in order to converge by iteration on the gas density profile $\rho(r)$ consistent with the observed emission. For the simple specific choice of $\rho(r)$ given by Eq. (6) with $\beta = \frac{1}{2}$, we have at large radii ($r \gg r_0$) for the case where $M(r)$ increases linearly with radius $M(r) \approx \bar{M}(r/r_0)$:

$$T(r) \approx c_1 \left(\frac{r}{r_{stag}}\right)^{3/2} + c_2 \left[1 - \left(\frac{r}{r_{stag}}\right)^{3/2}\right] \tag{8}$$

which shows a positive gradient if $c_1 > c_2$. The case $c_1 = c_2$ defines a critical value for the external pressure p_{ext}:

$$p_{ext}^{crit} = \rho_0 \frac{\mu m_p G \bar{M}}{k r_0} \left(\frac{r_0}{r_{stag}}\right)^{3/2}. \tag{9}$$

The quantity p_{ext}^{crit} represents the value of the external pressure of an isothermal model in virial equilibrium. For the model E the value of p_{ext}^{crit} is about 1000 K cm^{-3}.

Following the prescriptions given in Eqs. (6)-(7) we have calculated a number of hydrostatic models for the temperature profiles, based on the stellar dynamical models and the values of the intracluster pressure assumed in the cooling flow models described in Table 2. The behavior of these models is shown in Fig. 4. In the last column of Table 2 we list the emission-weighted temperatures of the hydrostatic models for comparison with the corresponding cooling flow models.

Thus the general conclusion, that the predicted temperature profiles seem to be essentially independent on the amount of dark matter associated with the stellar dynamical model, holds unaltered even in this semi-empirical test that incorporates the whole X-ray emission profile.

5. Conclusions

Currently available X-ray data do not allow for an accurate determination of the temperature profile for the hot gas that is thought to be present in bright elliptical galaxies. The physics of such interstellar gas is quite complex, given the uncertainties on its chemical composition, on the relevant heating sources, on the geometry of the gas distribution and on the role of the intracluster medium.

The purpose of this paper was not to study all the issues that can be raised in modeling the X-ray emission from elliptical galaxies, nor to discuss in detail the X-ray data from specific sources. Rather, we have focused on the question whether X-ray data can really discriminate models with different amounts of dark matter, i.e. on the effectiveness of the X-ray modeling as a diagnostic tool for the galactic potential well. To this purpose, we have referred to one simple class of standard cooling flow models, which, in spite of various limitations (e.g. they do not include the possibility of "localized" heating sources and do not address the issues raised by the observed correlation between X-ray emission and optical isophotal shapes (see Bender et al. 1989)), appear to provide a promising framework for the interpretation of X-ray data of bright sources. We have shown that dynamical models characterized by a very wide range in the amount of dark matter present, *if constrained by the same set of accurate and extended stellar dynamical data* (out to $\approx R_e$), all lead to remarkably similar X-ray profiles (out to $\approx 7R_e$). In fact, the temperature profile, which is not well determined observationally, does not change significantly because of the requirement that the various models for the gravitational potential, with or without dark matter, must be consistent with the observed stellar dispersion profile.

Special attention has been paid to the case of NGC 4472, which is probably the elliptical galaxy for which the best stellar dynamical data and modeling are available. The analysis shows that the relatively high values of the temperature (≈ 2 keV) reported by *Ginga* can be understood if a sizable, probably unrealistic, value for the intracluster pressure p_{ext} is assumed. A more reasonable explanation could be that the value of the intracluster pressure is moderate ($p_{ext} \approx 10\,000$ Kcm^{-3}) and the temperature reported by *Ginga* overestimates the gas temperature, as a result, e.g., of contamination by cluster emission

© European Southern Observatory • Provided by the NASA Astrophysics Data System

1993A&A...271..381B

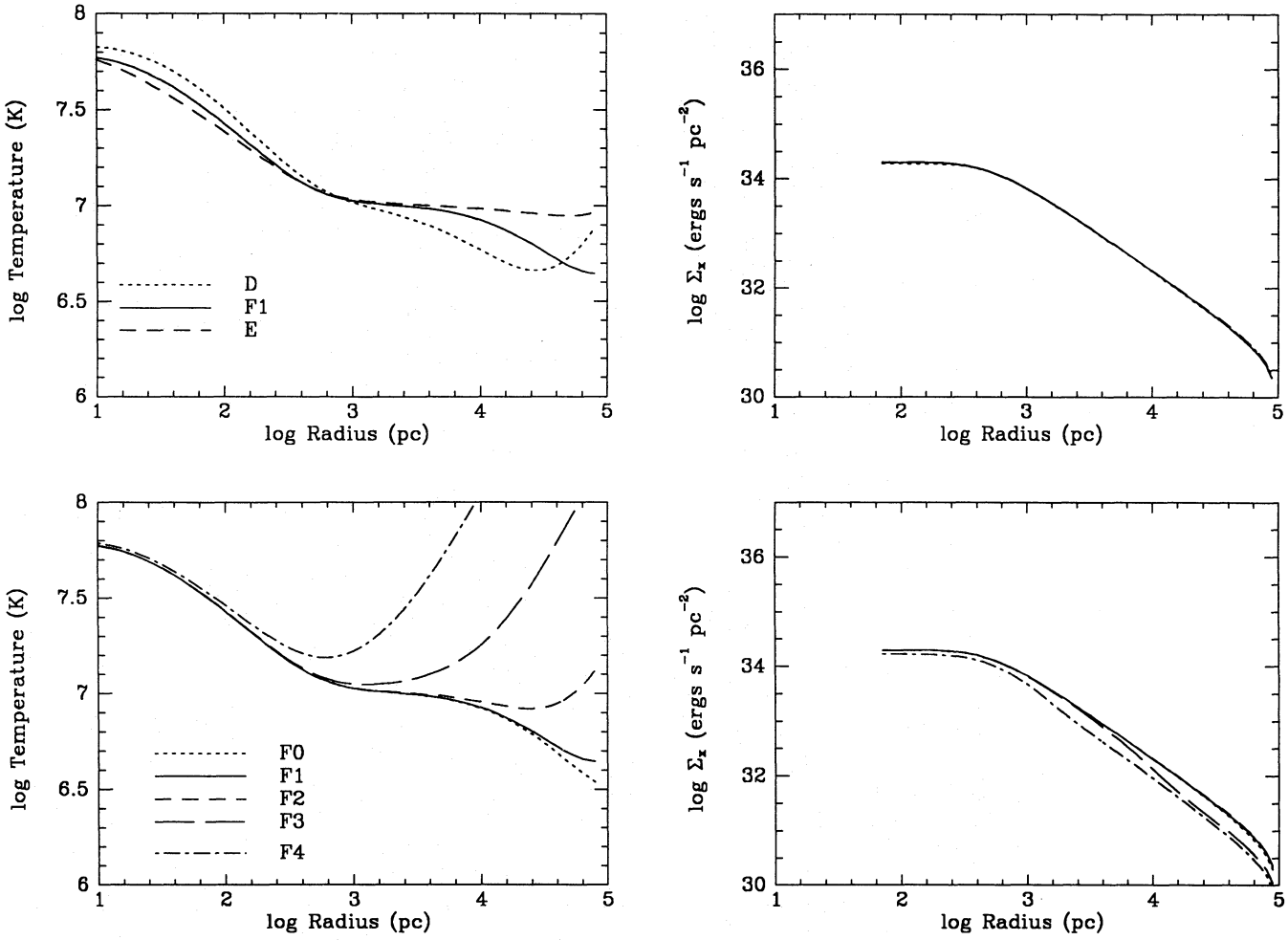

Fig. 4. Same as in Fig. 2, but for the corresponding hydrostatic models (see Table 2)

and/or by discrete sources with a harder spectrum. On the other hand, we find no reason to invoke large amounts of dark matter (which would be inconsistent with the available stellar dynamical data, Loewenstein 1992).

On this basis, we also conclude that so far the best evidence for dark matter in ellipticals does not derive from X-rays, but, especially for NGC 4472, from stellar dynamical data.

More accurate X-ray temperature profiles for elliptical galaxies are clearly desired and are going to be soon obtained with the use of improved X-ray telescopes. Still it seems that the difficulties in extracting from these data the actual temperature profiles for the interstellar *gas within the galaxy* and the complexity of the modeling of such hot gas make it very hard to obtain an unambiguous independent determination of the galactic potential well from the X-ray data. This paper suggests that any conclusion drawn in this respect should be taken with caution and checked to be consistent with the available stellar dynamical data, which have been shown here to impose severe constraints on the X-ray emission and temperature profiles of the interstellar gas.

Acknowledgements. We would like to thank Craig L. Sarazin for useful suggestions and especially for providing us with a copy of his code for the calculation of the emission profiles of an X-ray emitting gas with specified temperature and density for comparison with the observations, and G. Fabbiano and A. Renzini for interesting comments and conversations. This work was partially supported by MURST and CNR of Italy.

Appendix A: power law fits to cooling flow profiles

Let us assume that the gas density and temperature follow, locally, a power law $\rho \sim r^{-\beta}$, $T \sim r^{-\gamma}$ and concentrate on the region where the equilibrium is approximately hydrostatic. Then we find

$$\frac{kT}{\mu m_p}(\beta+\gamma) \approx \frac{GM(r)}{r} \tag{A1}$$

which is a constant when M(r) grows linearly with radius. In particular, for $r \ll r_L$, we have in our models $M(r) \approx (M_L/2r_L)r$, and thus:

$$kT \approx \frac{\mu m_p}{\beta}\frac{GM_L}{2r_L} \approx \frac{\mu m_p}{\beta}\sigma_*^2(0). \tag{A2}$$

© European Southern Observatory • Provided by the NASA Astrophysics Data System

1993A&A...271..381B

In the quasi-hydrostatic, quasi-isothermal limit here considered the energy equation becomes:

$$\frac{kT}{\mu m_p}\frac{\alpha}{4\pi}\frac{\left[M_*(r_{stag})-M_*(r)\right]}{r^2\rho(r)}\frac{\mathrm{d}\rho}{\mathrm{d}r} \approx -\rho^2\Lambda(T)+\frac{3\alpha}{2\mu m_p}\rho_*\left(kT_{in}-\frac{5}{3}kT\right) \quad \text{(A3)}$$

where we have made use of the continuity equation (4).

We can thus identify an *inner* region where the radiation losses "drive" the left hand side, so that by replacing $\left[M_*(r_{stag})-M_*(r)\right]$ by M_L we obtain:

$$\rho \approx \left(\frac{3}{8\pi}\frac{\alpha M_L}{\Lambda(T)}\frac{kT}{\mu m_p}\right)^{1/2} r^{-3/2}. \quad \text{(A4)}$$

Since the models are nearly isothermal, and the cooling function $\Lambda(T)$ changes only by a factor of two in the temperature range $5\cdot 10^6$ K $\lesssim$ T $\lesssim 10^8$ K, the X-ray brightness profile (integrated along the line of sight) associated with the above behavior of the gas density is $I_X(R)\propto R^{-2}$. From Eq. (A4) we note that the slope of the gas density profile, and thus of the related X-ray emission profile, does not depend on the detailed shape of the potential well nor on the value of the external pressure p_{ext}, consistent with the results shown in Fig. 2. In particular, it is explained why such profiles are not sensitive to the amount of dark matter present.

If we now recall that $T\sim M_L$, Eq. (A4) is found to imply for the *total* X-ray luminosity L_X the scaling $L_X\propto M_L^2\propto L_B^2$, where the mass-to-light ratio M_L/L_B has been assumed to be fairly constant from galaxy to galaxy. Therefore, these models are consistent with the empirical correlation $L_X\sim L_B^{1.42-2.11}$ (CFT) and with the steeper, more recent correlation $L_X\sim L_B^{1.9-2.2}$ found by Donnelly et al. (1990; see also White & Sarazin 1991). In this argument the use of Eq. (A4) is well justified, since the *total* X-ray emission is dominated by the contribution of the *inner* region.

At a radius r_t, with $r_t\approx r_L/(T_{in}/T-5/3)$ the contribution of supernova heating becomes of the order of the potential energy release. In the *outer* region $r>r_t$, supernova heating dominates and, if $T_{in}\gg\frac{5}{3}T$, we have

$$\Lambda(T)\rho^2\approx\frac{3}{2}\alpha\rho_*\frac{kT_{in}}{\mu m_p} \quad \text{(A5)}$$

so that $\rho\sim r^{-2}$ (since our models are characterized by $\rho_*\sim r^{-4}$ for $r>r_L$), but some changes are expected if the external pressure is increased significantly. This relation, $\rho^2\sim\rho_*$, is consistent with the observed matching of the X-ray and optical luminosity profiles.

The results of this simple analytical discussion appear to explain the computed profiles even beyond the strict limits of the developed asymptotic analysis. In fact, the gas density profiles of our models are well represented by a power law throughout the galaxy. For model F1, the transition radius occurs at $r_t\approx 8$ kpc. At $r\approx 2$ kpc, the supernova heating is only one third of the potential energy contribution; at $r\approx 20$ kpc, it has grown up to three times the Φ-term.

Appendix B: a viscous model

In this Appendix we would like to comment briefly on the regularity condition that is imposed at the inner sonic radius r_{son}.

The basic momentum and energy transport equations are modified by the effect of finite shear viscosity η and of thermal conductivity κ in the following way. A viscous term

$$f_\eta=-\frac{1}{r^2}\frac{\mathrm{d}}{\mathrm{d}r}\left[r^2\frac{4}{3}\eta r\frac{\mathrm{d}}{\mathrm{d}r}\left(\frac{u}{r}\right)\right] \quad \text{(B1)}$$

should be added to the left hand side of Eq. (2), while a dissipation term of the form

$$d_{\kappa,\eta}=-\frac{1}{r^2}\frac{\mathrm{d}}{\mathrm{d}r}\left[r^2\left(\kappa\frac{\mathrm{d}T}{\mathrm{d}r}+\frac{4}{3}\eta r u\frac{\mathrm{d}}{\mathrm{d}r}\left(\frac{u}{r}\right)\right)\right] \quad \text{(B2)}$$

should be added to the left-hand-side of Eq. (3). Estimates of η and κ based on microscopic theory, and the absence of sizable temperature and velocity gradients throughout most of the galaxy, would suggest that viscosity and thermal conductivity could well be ignored in the models. On the other hand, by analogy with other problems in plasma astrophysics, one should be ready to accept the possibility that collective modes can be responsible for unexpectedly large ("anomalous") transport processes. Here, effects of this kind may help regularize the cooling flow equations at the sonic radius. In fact, the sonic singularity present in the set of Eqs. (1)-(3) is removed by the higher derivative viscous terms much like in a boundary layer problem. For the solar wind a similar result had been shown to hold by Whang et al. (1965) who constructed a viscous model for the heliosphere.

References

Awaki, H., Koyama, K., Kurieda, H., Takono, S., Tawara, Y., Ohashi, T. 1991, ApJ 366, 88

Balbus, S.A. 1988, ApJ 328, 395

Bender, R., Surma, P., Döbereiner, S., Möllenhoff, C., Madejsky, R. 1989, A&A 217, 35

Bertin, G., Saglia, R.P., Stiavelli, M. 1992, ApJ 384, 423 (BSS)

Canizares, C.R., Fabbiano, G., Trinchieri, G. 1987, ApJ 312, 503 (CFT)

Ciotti, L., d'Ercole, A., Pellegrini, S., Renzini, A. 1991, ApJ 376, 380

Davies, R.L., Birkinshaw, M. 1988, ApJS 68, 409

Donnelly, R.H., Faber, S.M., O'Connell, R.M. 1990, ApJ 354, 52

Fabbiano, G. 1989, ARA&A 27, 87

Fabian, A.C., Nulsen, P.E.J. 1977, MNRAS 180, 479

Fabian, A.C., Thomas, P.A., Fall, S.M., White, R.E.III 1986, MNRAS 221, 1049

Fabricant, D., Gorenstein, P. 1983, ApJ 267, 535

Forman, W., Jones, C., Tucker, W. 1985, ApJ 293, 102

Forman, W., Schwarz, J., Jones, C., Liller, W., Fabian, A.C. 1979, ApJ 234, L27

Kim, D-W., Fabbiano, G., Eskridge, P.B. 1992, preprint.

Loewenstein, M. 1992, ApJ 384, 474

Loewenstein, M., Mathews, W.G. 1987, ApJ 319, 614

Mathews, W.G., Bregman, J.N. 1978, ApJ 224, 308

Saglia, R.P., Bertin, G., Bertola, F., Danziger, J., Dejonghe, H., Sadler, E., Stiavelli, M., De Zeeuw, T., Zeilinger, W.W. 1993, ApJ 403, 567

Saglia, R.P., Bertin, G., Stiavelli, M., 1992, ApJ 384, 433 (SBS)

© European Southern Observatory • Provided by the NASA Astrophysics Data System

1993A&A...271..381B

Sancisi, R., van Albada, T.S. 1987, in: Observational Cosmology, eds. A. Hewitt et al., Reidel, Dordrecht, p. 699.
Sarazin, C.L. 1987, in: Structure and Dynamics of Elliptical Galaxies, ed. P.T. de Zeeuw, Reidel, Dordrecht, p. 179.
Sarazin, C.L., 1990, in: The Interstellar Medium in Galaxies, eds. H. A. Thronson, Jr, and J. M. Shull, Kluwer, p. 201
Sarazin, C.L., Ashe, G.A. 1989, ApJ 345, 22
Sarazin, C.L., White, R.E. III 1987, ApJ 320, 32
Sarazin, C.L., White, R.E III 1988, ApJ 331, 102
Takano, S., Awaki, H., Koyama, K., Kunieda, H., Tawara, Y., Yamauchi, S., Makishima, K., Ohashi, T. 1989, Nature 340, 289
Thomas, P.A. 1986, MNRAS 220, 949
Trinchieri, G., Fabbiano, G., Canizares, C.R. 1986, ApJ 310, 637
van Albada, T.S., Bahcall, J., Begeman, K., Sancisi, R. 1985, ApJ 295, 305
Vedder, P.W., Trester, J.J., Canizares, C.R. 1988, ApJ 332, 725
Whang, Y.C., Liu, C.K., Chang, C.C. 1965, ApJ 145, 255
White, R.E. III, Sarazin, C.L. 1991, ApJ 367, 476

This article was processed by the author using Springer-Verlag LaTeX A&A style file version 3.

© European Southern Observatory • Provided by the NASA Astrophysics Data System